Journal of Industrial and Engineering Chemistry 122 (2023) 341–348

Contents lists available at ScienceDirect

Journal of Industrial and Engineering Chemistry

journal homepage: www.elsevier.com/locate/jiec

Exploring the use of butadiene rubbers as a binder in composite cathodes for all-solid-state lithium batteries

Young-Jun Lee, Seung-Bo Hong, Dong-Won Kim *

Department of Chemical Engineering, Hanyang University, Seoul 04763, Republic of Korea

ARTICLE INFO

Article history:
Received 17 January 2023
Revised 16 February 2023
Accepted 21 February 2023
Available online 25 February 2023

Keywords:
All-solid-state lithium battery
Sulfide solid electrolyte
Polymer binder
Composite cathode
Wet-slurry process

ABSTRACT

Among the various next-generation battery systems, all-solid-state lithium batteries (ASSLBs) employing sulfide-based solid electrolytes have garnered considerable attention because of their high energy density and enhanced safety compared to conventional lithium-ion batteries (LIBs) with liquid electrolytes. The fabrication of composite cathodes for ASSLBs by the wet-slurry process is highly desirable, because it can be scaled into a large sheet and be applied to the established slurry-processed electrode manufacturing technology of LIBs. A polymer binder in the composite cathode is an important component for maintaining good interfacial contacts among the electrode components (active material, solid electrolyte, and conducting carbon) during charge and discharge cycles. In this study, we used polybutadiene and acrylonitrile-butadiene rubbers (NBR) with different acrylonitrile (AN) contents as a polymer binder in the composite cathode. Our results demonstrated that a composite cathode employing NBR with 25 wt.% AN (NBR25) showed good elastic properties and superior adhesion without the large deterioration of interfacial contacts during cycling. The solid-state Li-In/Li_6PS_5Cl/$LiNi_{0.7}Co_{0.1}Mn_{0.2}O_2$ cell assembled with the composite cathode employing NBR25 exhibited an initial discharge capacity of 149.0 mAh g^{-1} with good capacity retention at 0.2 C and 25 °C.

Introduction

Many countries have implemented various eco-friendly policies to reduce carbon emissions and solve global warming problems. Therefore, the number of internal combustion engine (ICE) vehicles emitting greenhouse gases, such as CO_2, must be reduced; thus, many ICE-based automobiles have gradually been converted to electric vehicles (EVs) [1]. The development of rechargeable batteries with high energy densities and enhanced safety is essential for the commercialization of EVs. However, conventional lithium-ion batteries employing flammable liquid electrolytes have intrinsic safety concerns, such as fires and explosions under abnormal conditions [2,3]. To solve these safety issues, all-solid-state lithium batteries (ASSLBs) employing nonflammable solid electrolytes have garnered considerable attention owing to their high energy density and enhanced safety [4–6].

Solid-state electrolytes can be classified as polymers, oxides, and sulfides. Among them, sulfide-based electrolytes, such as Li_2S–P_2S_5, $Li_7P_3S_{11}$, $Li_{10}GeP_2S_{12}$ (thio-LISICON), and Li_6PS_5X (X = Cl, Br, I; argyrodite), are promising electrolyte systems for ASSLBs because of their high ionic conductivity (~10^{-2} S cm^{-1}) comparable to that of liquid electrolytes. They also have high ductility, which enables the intimate interfacial contacts of inorganic particles without sintering at high temperature [4,7–14]. Nevertheless, many technical issues related to the fabrication of composite cathodes hinder the successful development of ASSLBs. The composite cathode usually undergoes a large volume change during the charge and discharge cycles, which deteriorates the interfacial contact among the active material, solid electrolyte, and conducting carbon with cycling, thereby degrading the cell performance. Therefore, an appropriate amount of polymer binder is necessary to maintain the interfacial contact and ensure that the cathode components adhere to the current collector. However, the conventional wet-slurry process used in fabricating the composite cathode for ASSLBs has some challenges, such as the increase in electrical resistance due to the presence of a polymer binder in the composite cathode and the poor solubility of the polymer binder in nonpolar solvents [15–17]. It is noticeable that nonpolar or less polar solvents should be used in preparing the electrode slurry, because sulfide-based electrolytes easily react with highly polar solvents, such as N-methyl pyrrolidone [18,19]. Accordingly, the selection of a polymer binder that can be dissolved in less polar solvents is crucial for providing facile elec-

* Corresponding author.
E-mail address: dongwonkim@hanyang.ac.kr (D.-W. Kim).

https://doi.org/10.1016/j.jiec.2023.02.034
1226-086X/

tron/ion pathways and maintaining good interfacial contacts among the electrode components during cycling.

In this study, we used polybutadiene (PBD) and acrylonitrile-butadiene rubber (NBR) with different acrylonitrile (AN) contents (25 and 37 wt.% nitrile) as a polymer binder in preparing the composite cathode through the wet-slurry process. PBD is an elastomer with high elasticity and flexibility owing to its low glass transition temperature (T_g). It also dissolves well in nonpolar solvents. NBR is an elastomeric copolymer comprising repeating units of acrylonitrile and butadiene. In NBR, nitrile (-C≡N) groups can induce ion–dipole inter-

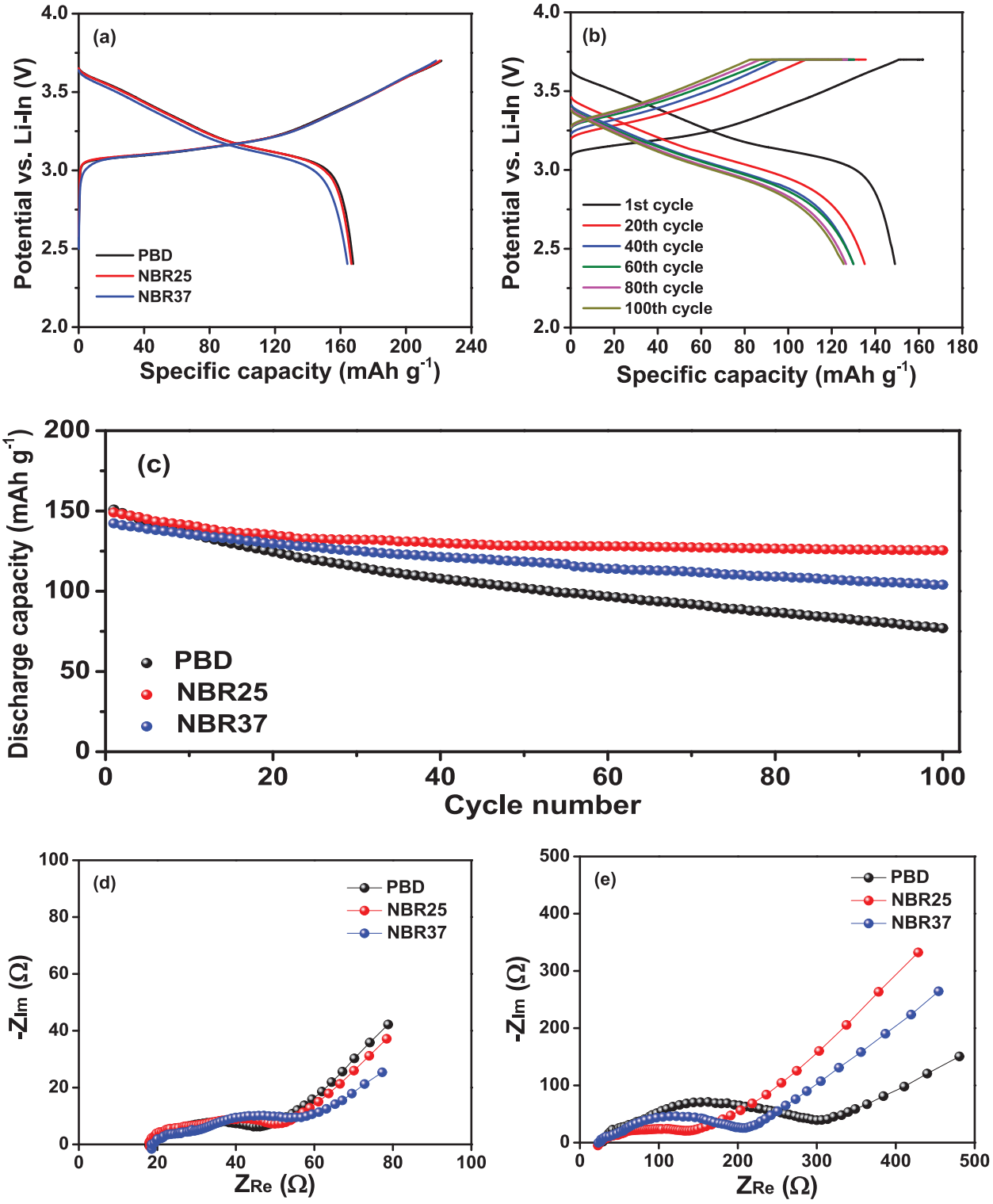

Fig. 1. (a) Voltage profiles of all-solid-state cells with three different binders during the first pre-conditioning cycle at a current rate of 0.05 C. (b) Charge and discharge curves of the cell prepared with NBR25 at a current rate of 0.2 C. (c) Cycling performance of all-solid-state cells with different binders at a current rate of 0.2 C. The AC impedance spectra of all-solid-state cells with different binders (d) before and (e) after 100 cycles.

actions with the active cathode material and sulfide electrolyte in the composite cathode, resulting in enhanced adhesion of the electrode components. In contrast, a high AN content reduces the flexibility and elasticity of the composite cathode owing to the high glass transition temperature of polyacrylonitrile. Herein, we prepared the composited cathodes comprising $LiNi_{0.7}Co_{0.1}Mn_{0.2}O_2$, Li_6PS_5Cl (LPSCl, argyrodite), conducting carbon, and different types of polymer binders. All-solid-state Li-In/Li_6PS_5Cl/$LiNi_{0.7}Co_{0.1}Mn_{0.2}O_2$ cells were then assembled with different composite cathodes and their electrochemical performance was evaluated to investigate the effect of the polymer binder on the cycling performance of the cells.

Experimental

Materials

N-butyl butyrate (BB) and benzyl acetate (BA) were purchased from Alfa Aesar and Sigma-Aldrich, respectively. PBD and NBR (NBR37, 37 wt.% nitrile) were purchased from Sigma Aldrich and the other NBR (NBR25, 25 wt.% nitrile) was kindly supplied from Kumho Petrochemical Co., Ltd. $LiNi_{0.7}Co_{0.1}Mn_{0.2}O_2$ (NCM712, d_{50} = 10 μm) was supplied by L&F Co., Ltd., and used after vacuum drying at 100 °C for 24 h. LPSCl (d_{50} = 1 μm) was purchased from Jeong Kwan Co., Ltd. Lithium metal and indium foil were purchased from Honjo Metal Co. Ltd. and Nilaco, respectively.

Electrode preparation and cell assembly

The binder solution was prepared by dissolving 5.0 wt.% of the polymer binder (PBD, NBR25, and NBR37) in the mixed solvent of BB/BA (1:1 by weight). A coating slurry comprising NCM712, LPSCl, Super-P carbon, and binder (70:26:3:1 by weight) in the solvent was homogeneously mixed using a planetary centrifugal mixer (Thinky Mixer AR-100). The resulting slurry was then cast onto a carbon-coated aluminum foil with a doctor blade and vacuum-dried at 80 °C for 24 h to remove residual solvents. As shown in **Fig. S1**, all the components in the composite cathode were well adhered to the aluminum current collector without detachment after punching, and the obtained composite cathodes were flexible due to the presence of elastic polymer binder. The mass loading of NCM712 in the

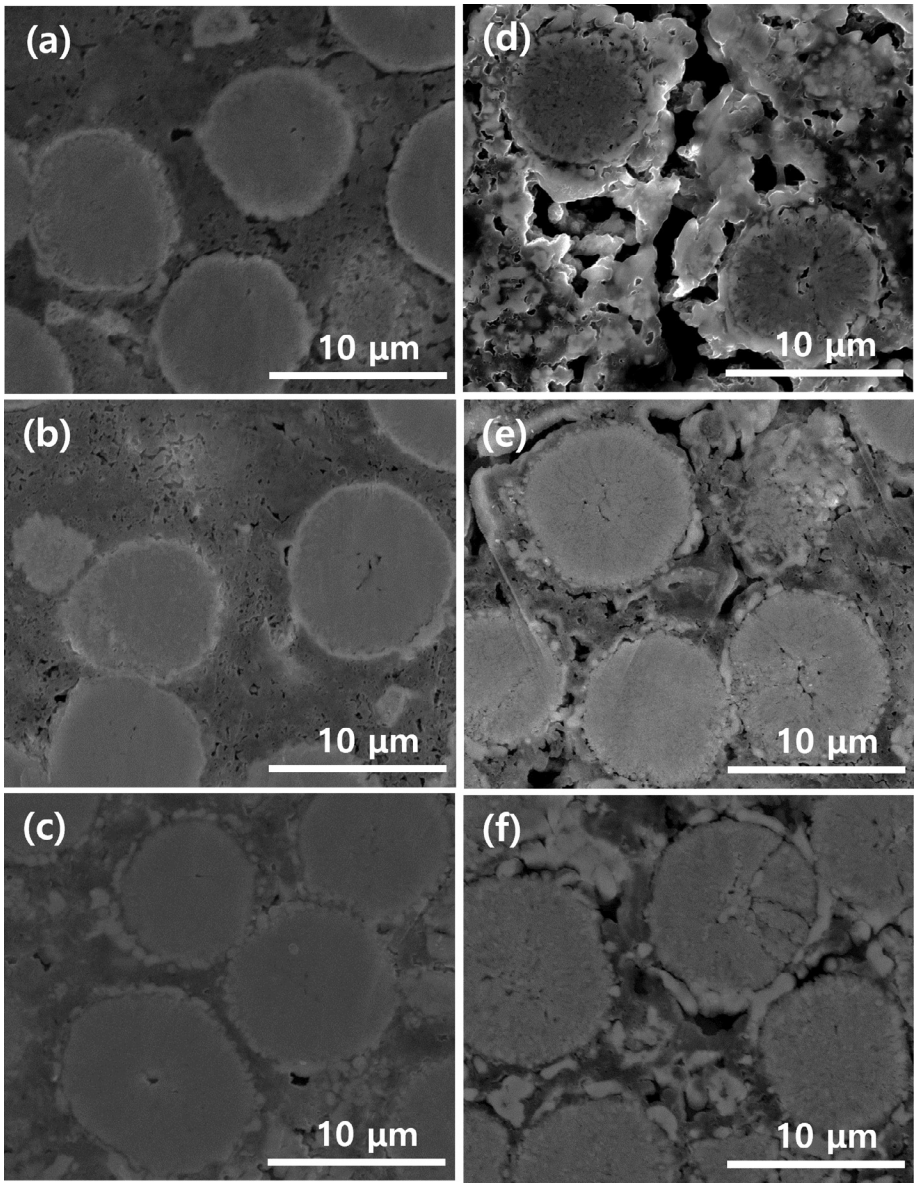

Fig. 2. Cross-sectional SEM images of the composite cathodes prepared with different binders (a-c) before and (d-f) after 100 cycles. (a),(d) PBD, (b),(e) NBR25, and (c),(f) NBR37.

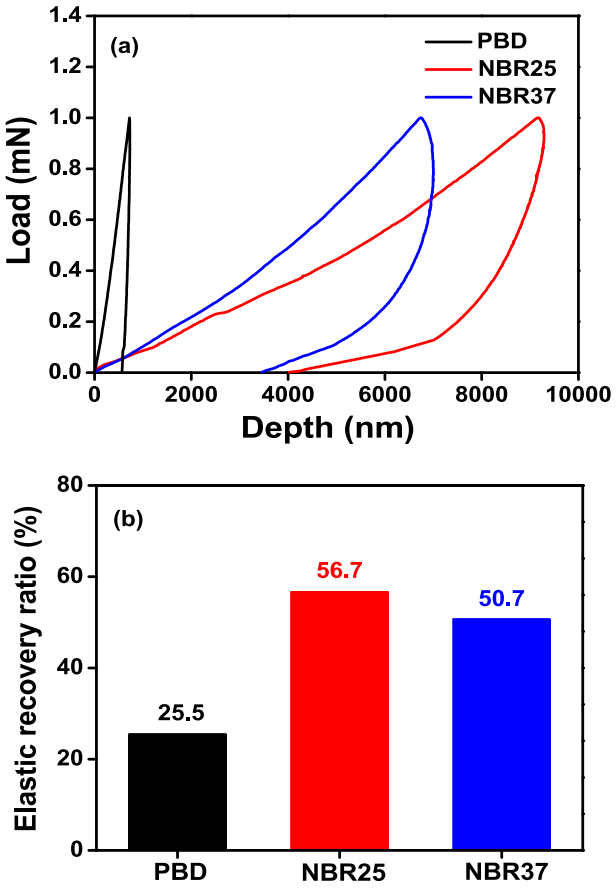

Fig. 3. (a) Nanoindentation load-depth curves of the composite cathodes prepared with different binders at the maximum load of 1.0 mN and (b) elastic recovery ratio of the composite cathodes with different binders.

composite cathode was approximately 14 mg cm^{-2}. A solid electrolyte pellet with a thickness of 800 μm was prepared by cold pressing 100 mg of LPSCl at 300 MPa. A thick solid electrolyte pellet was used in this study, because the solid electrolyte was too brittle to prepare a thin solid pellet. The composite cathode was then placed onto a pelletized solid electrolyte and pressed under a constant load of 420 MPa. The Li-In foil was then placed on the other side of the solid electrolyte as an anode, and the cell was pressed at a torque of 11 Nm, corresponding to the stack pressure of 75 MPa. The molar ratio of Li and In in the anode was 0.5 : 1.0. All the above processes were conducted in a glove box (MBRAUN) filled with highly pure argon gas.

Characterization and measurements

The chemical structures of the polymer binders were confirmed by ^{1}H NMR spectroscopy using a VNMRS 600 MHz spectrometer and Fourier transform infrared (FT-IR) spectroscopy between 800 and 2400 cm^{-1} using a Nicolet iS50 spectrometer. X-ray diffraction (XRD, MiniFlex 600 X-ray diffractometer) was used to investigate the crystal structures of the LPSCl, NCM and composite cathodes with different binders. The cross-sectional morphologies of the composite cathodes were examined before and after cycling by scanning electron microscopy (SEM) using a Nova NanoSEM 450 instrument. The SEM images were processed using the ImageJ software to estimate the void fraction in the composite cathode. Nanoindentation was conducted using a NanoTest NTX. The adhesion properties of the composite cathode were investigated using a surface and interfacial cutting analysis system (SAICAS, Daipla Wintes). The chemical composition of the products formed on the composite cathode after cycling was investigated using X-ray photoelectron spectroscopy (XPS, VG Multilab ESCA system 220i). All spectra were fitted with a Lorentzian–Gaussian peak fit function and linear-type background using the XPSPEAK41 software.

Electrochemical measurement

Electrochemical impedance spectroscopy was conducted using a Zahner Electrik IM6 impedance analyzer at an amplitude of 5 mV in the frequency range of 1 mHz to 1 MHz. The cycling performance of solid-state Li-In/Li_6PS_5Cl/$LiNi_{0.7}Co_{0.1}Mn_{0.2}O_2$ cells was evaluated using a battery cycler (WBCS 3000, Wonatech) at 25 °C. The cell was pre-cycled twice in the voltage range of 2.4–3.7 V (vs. Li-In) at a current rate of 0.05 C. After the pre-conditioning cycles, it was charged to 3.7 V at a constant current of 0.2 C and further charged at constant voltage until the value of the current reached 10% of the charging current. The cell was then discharged to a cut-off voltage of 2.4 V at a current of 0.2 C (1 C = 2.5 mA cm^{-2}). The rate capability of the cells was investigated at current rates ranging from 0.1 to 1.0 C.

Results and discussion

The chemical structures of the polymer binders used in this study were confirmed by ^{1}H NMR and FT-IR spectroscopy. **Fig. S2a and S2b** show the chemical structures and ^{1}H NMR spectra of PBD, NBR25, and NBR37, respectively. As shown in **Fig. S2b**, NBR exhibits additional proton peaks at 1.66 and 2.59 ppm, corresponding to the methylene (-CH_2-, H_D) and methine (-CHCN-, H_C) protons, respectively. From the peak intensities, the molar ratios of AN in NBR25 and NBR37 were calculated to be 32 and 48%, respectively, which are consistent with 25 and 37 wt.% nitrile, respectively. According to the FTIR spectra shown in **Fig. S2c**, all polymer binders were characterized by small peaks at 1,640 and 1,670 cm^{-1}, which can be assigned to C=C double bonds in the butadiene unit. NBR showed an additional peak corresponding to nitrile (-C≡N) groups at approximately 2,235 cm^{-1}. These results confirm that the polymer binders had the expected structure without any impurities. The polymer binders used in this study showed different solubilities in organic solvents. PBD was not dissolved in BA alone, and NBR37 was insoluble in BB alone. However, all polymer binders could easily be dissolved in a mixed solvent of BA and BB at a weight ratio of 1:1, as shown in **Fig. S3**.

Based on previous reports, the crystal structure of LPSCl treated with polar organic solvents experienced serious collapse, leading to a decrease in the ionic conductivity of LPSCl and the deterioration of cell performance [15,18]. To investigate the change in the crystalline structure of LPSCl caused by organic solvents, we conducted XRD analysis of LPSCl before and after treatment with different solvents. LPSCl was immersed in each solvent for 48 h and then vacuum-dried to remove the solvent at 80 °C for 24 h. As shown in **Fig. S4**, the XRD patterns of LPSCl treated with different solvents were consistent with that of pristine LPSCl, indicating that LPSCl was chemically stable in the organic solvents used in this study. Based on the solubility test and XRD analysis, a mixed solvent of BA and BB (1:1 by weight) was used to prepare a wet slurry for the composite cathode. The cyclic voltammograms of the LPSCl-binder composites in **Fig. S5** confirm that all the binders investigated in this study are electrochemically stable in the voltage range of 1.0 to 3.7 V vs. Li-In. From the XRD patterns of the composite cathodes with different binders (**Fig. S6**), it is confirmed that LPSCl has good chemical stability toward organic solvents and NCM without any side reactions and degradation during the preparation of composite cathode.

The cycling performance of the solid-state Li-In/Li_6PS_5Cl/$LiNi_{0.7}Co_{0.1}Mn_{0.2}O_2$ cells assembled with different composite cathodes

was evaluated at 0.2 C and 25 °C. Each cell was named based on the polymer binder used in the composite cathode. For example, the cell assembled with the composite cathode using NBR25 was referred to as the NBR25 cell. Prior to the cycling test, the cells were subjected twice to two preconditioning cycles at a current of 0.05 C. The voltage profiles of the cell obtained in the first preconditioning cycle are shown in Fig. 1**a**. All the cells exhibited similar voltage profiles and exhibited discharge capacities of 164.2–167.7 mAh g^{-1} at a current rate of 0.05 C. Fig. 1**b** and **Fig. S7** show the charge and discharge curves of the cells employing different binders at a current of 0.2 C. The PBD and NBR37 cells exhibited the highest and lowest initial discharge capacities of 150.8 and 142.2 mAh g^{-1}, respectively. Considering the cycling stability, the NBR25 cell exhibited the best capacity retention of 84.2% after 100 cycles, whereas the PBD cell showed the worst cycling retention, as shown in Fig. 1**c**. AC impedance of the cells was measured before and after 100 cycles, and the results are shown in Fig. 1**d and 1e**, respectively. As given in the equivalent circuit in **Fig. S8**, the intercept on the real axis corresponds to the bulk resistance (R_b) of the sulfide electrolyte, and the depressed semicircle observed in the high- to low-frequency region can be ascribed to the interfacial resistances between the electrolyte and electrodes. In the depressed semicircle, the high-frequency semicircle can be assigned to Li^+ ion diffusion between the composite cathode and the solid electrolyte (R_{HF}), and the semicircle at low frequency is attributed to the charge transfer resistance (R_{ct}) [20–22]. The cells exhibited similar interfacial resistances before cycling, as shown in Fig. 1**d**. However, a large difference was observed in the interfacial resistance after 100 cycles. As depicted in Fig. 1**e**, the interfacial resistance decreased in the order of PBD > NBR37 > NBR25 after 100 cycles. The large increase in the interfacial resistance in the PBD cell may be related to the loss of interfacial contacts among NCM712, LPSCl, and conducting carbon because of the weak binding properties of the PBD binder during repeated cycling. This is because PBD does not have any polar functional groups to induce the ion–dipole interactions for strong adhesion with NCM712 and LPSCl in the composite cathode. In contrast, NBR25 and NBR37 contain nitrile groups that promote physical interactions with NCM712 and solid electrolytes (LPSCl) [23–25]. Meanwhile, the difference in the interfacial resistances in the NBR25 and NBR37 cells after cycling may originate from the difference in elastic properties between the two binders. The higher elasticity of

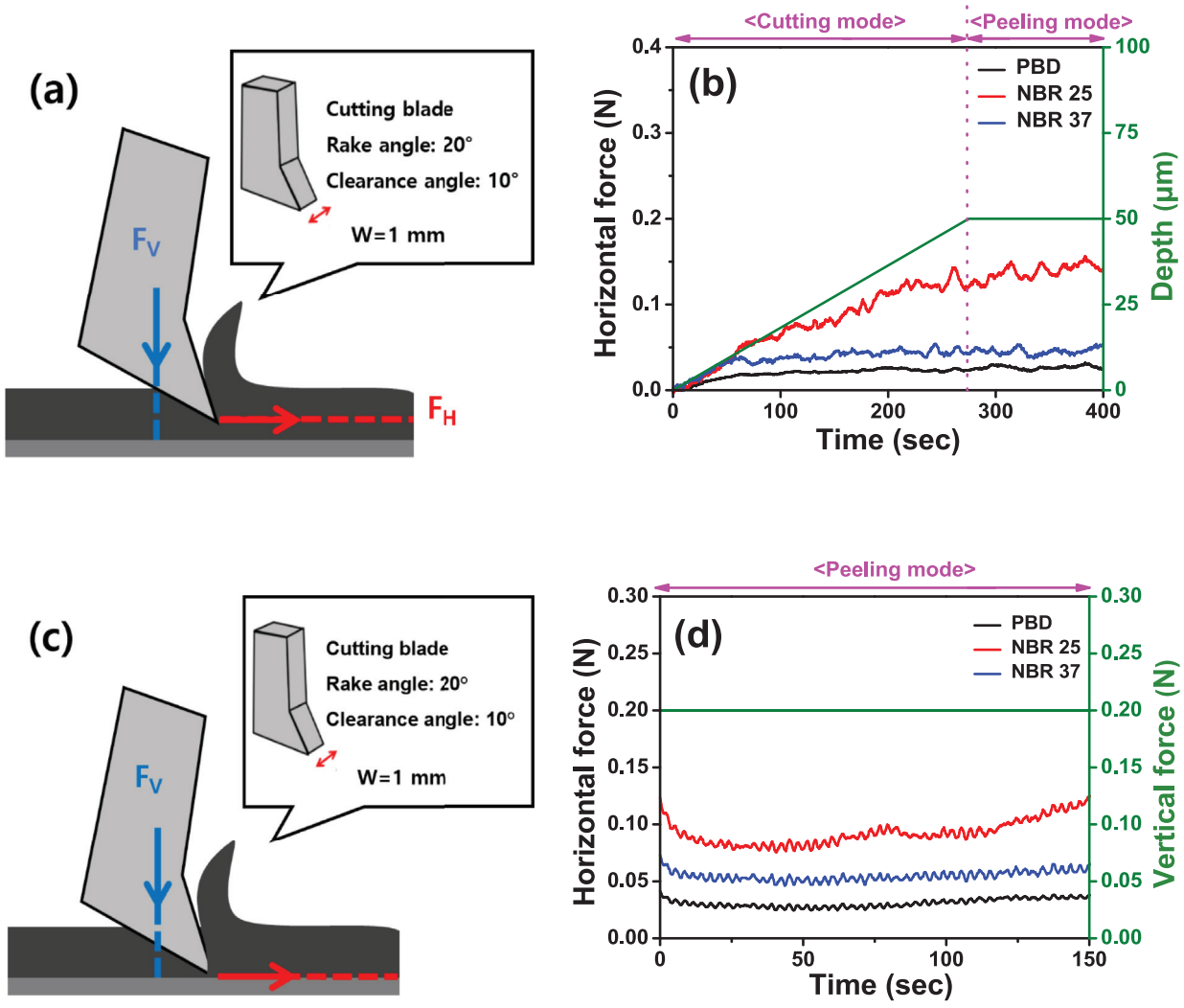

Fig. 4. Schematic illustrations of the SAICAS experiment at (a) constant velocity and (c) constant load modes. Forces required to cut and peel the composite cathode at (b) the middle part of the composite cathode and (d) the interface between the composite cathode and Al current collector.

NBR25 can relieve and withstand the mechanical stress induced by the volume expansion and contraction of NCM712 during cycling, thereby maintaining the interfacial contacts without the loss of electron and ion pathways in the composite cathode. After peeling off the solid electrolyte from the composite cathode prepared with NBR25, the chemical change occurring over the solid electrolyte pellet was investigated using XPS. As depicted in XPS spectra of **Fig. S9**, the solid electrolyte pellet exhibits no significant chemical changes before and after cycles, indicating the solid electrolyte is stable toward the NBR25.

To investigate the interfacial adhesion of the cathode components, cross-sectional SEM images of the composite cathode were obtained before and after cycling; the resulting SEM images are shown in Fig. 2. The left SEM images (Fig. 2**a–2c**) are of pristine composite cathodes, and the right ones (Fig. 2**d–2f**) are of composite cathodes after 100 cycles. Before cycling, all composite cathodes exhibited good interfacial contact between NCM712 and LPSCl. However, the composite cathode with PBD showed a large void space between the active material and solid electrolyte after cycling, and many cracks were observed within the NCM712 particles, which arise from the mechanical stress due the large volumetric changes of NCM712 during the repeated intercalation and deintercalation of Li^+ ions. Accordingly, the ion and electron pathways in the composite cathode with PBD were lost, thereby increasing the interfacial resistance and large capacity fading of the cell. In contrast, in the composite cathode employing NBR25, the interfacial contacts between the cathode components were well maintained with fewer voids after cycling. The void fraction in the composite cathodes was estimated using the ImageJ software [26]. **Fig. S10** shows the cross-sectional SEM images of the

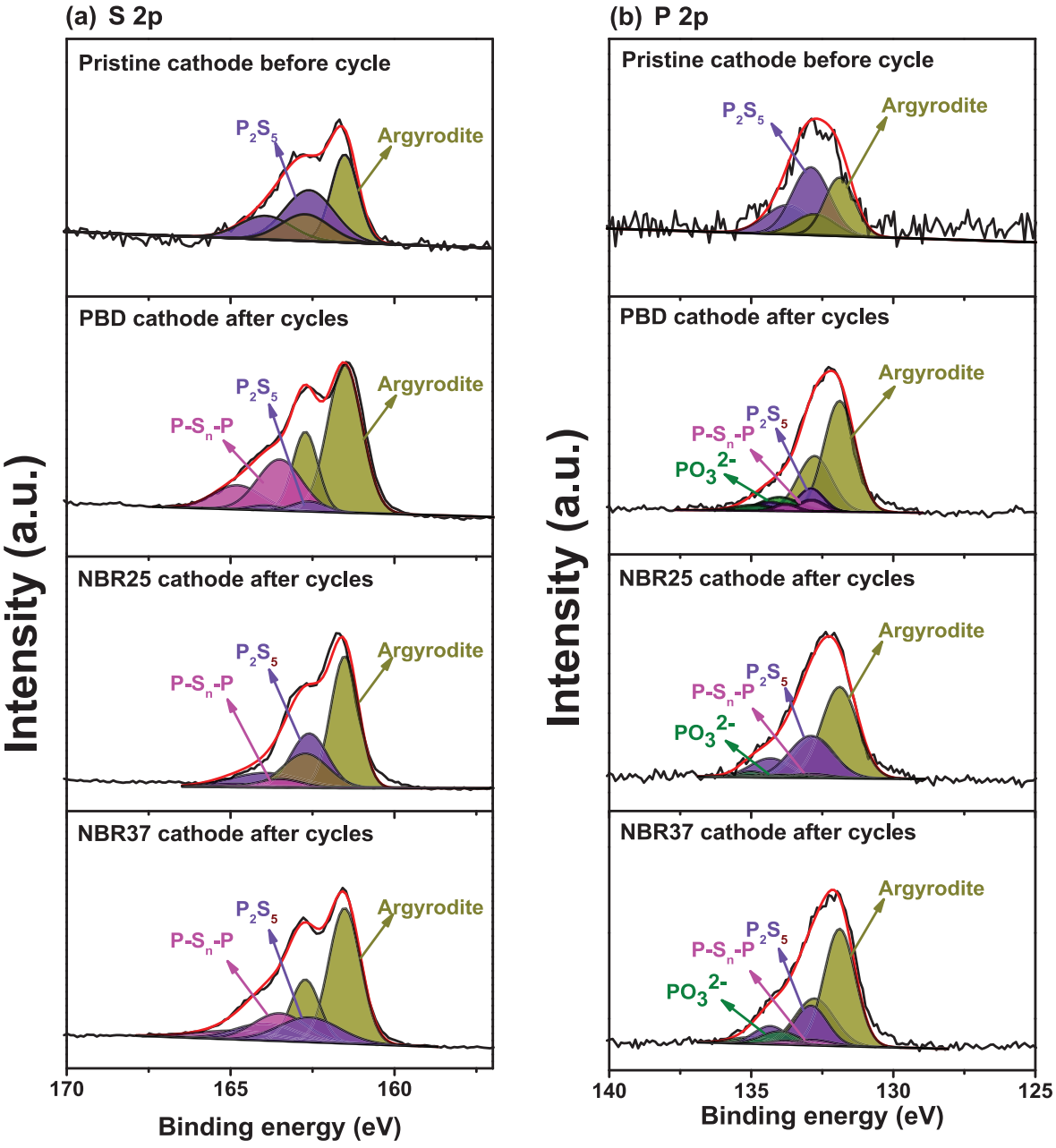

Fig. 5. XPS spectra of the composite cathodes with different binders before and after 100 cycles. (a) S 2p and (b) P 2p.

composite cathodes processed using the software. After cycling, the void fractions in composite cathodes prepared with PBD, NBR25, and NBR37 were calculated to be 15.9, 3.2, and 8.4%, respectively. As discussed previously, NBR25 can strongly adhere to NCM712 and LPSCl owing to the presence of polar nitrile groups and can accommodate the mechanical stress caused by the large volume change of NCM712 owing to its elastomeric properties, thereby maintaining good interfacial contacts. Notably, many cracks were observed in NCM particles in the composite cathode with NBR37, which can be attributed to the insufficient elastic properties of NBR37 that cannot withstand mechanical stress [27].

A nanoindentation experiment was conducted to measure the elastic recovery of composite cathodes prepared with different binders. The load versus depth curves of the different composite cathodes at a maximum load of 1 mN are shown in Fig. 3**a**. In this curve, the elastic recovery ratio is defined as the restored depth divided by the maximum penetration depth [28,29]. The elastic recovery ratios of the composite cathodes were estimated based on the nanoindentation curves and are shown in Fig. 3**b**. The composite cathode with PBD showed the smallest elastic recovery ratio as PBD does not have any polar groups that can effectively bind the cathode components, although PBD has intrinsically elastic properties. NBR37 has the least content of butadiene, making the composite cathode less elastic. Thus, the composite cathode with NBR25 exhibited the highest elastic recovery ratio due to its balanced adhesive and elastic properties.

The cohesive and adhesive strengths of the composite cathodes were investigated using SAICAS. The SAICAS experiment was conducted in two modes: constant velocity mode and constant load mode, as illustrated in Fig. 4**a and 4c**. In the constant velocity mode, the cutting blade cuts the composite cathode in the horizontal and vertical directions at speeds of 2 and 0.2 μm s^{-1}, respectively. When the cutting blade reaches the middle part of the composite cathode, it cuts the electrode only in the horizontal direction at a constant speed. The horizontal forces measured in the constant-velocity mode are shown in Fig. 4**b**. As shown in the figure, the composite cathode prepared with PBD exhibited the smallest force, implying that the composite cathode with PBD had poor cohesion properties [30]. In contrast, the composite cathode with NBR25 exhibited the largest cohesive strength. In the constant load mode, the cutting blade cuts between the composite cathode and aluminum current collector with the same force of 0.2 N, and the resulting horizontal forces are depicted in Fig. 4**d**. In this mode, the composite cathode containing NBR25 exhibited the highest adhesive force. Based on these SAICAS results, NBR25 was found to have the highest cohesive and adhesive strengths to effectively bind the cathode components, which is completely consistent with the cross-sectional SEM images (Fig. 2) and nanoindentation results (Fig. 3). Based on these results, the morphological changes in the interface between NCM712 and LPSCl in the composite cathode are schematically illustrated in **Fig. S11**. As the composite cathode prepared with NBR25 had an appropriate amount of AN groups to induce ion–dipole interactions and butadiene groups with high elasticity, it could withstand volumetric strain and maintain good interfacial contacts during repeated cycling.

During repeated cycling, the solid electrolyte (LPSCl) was oxidatively decomposed on the surface of the composite cathode. The decomposed products formed on the cathode after 100 cycles were investigated using XPS. The XPS spectra of the composite cathodes before and after cycling are shown in Fig. 5. The peaks corresponding to P-S_n-P and PO_3^{2-} can be clearly observed on the surface of the cycled composite cathodes, which are the oxidatively decomposed products of LPSCl at high voltage [31–35]. When the area of LPSCl was 1.0, the relative areas of the decomposed products were calculated and are shown in **Fig. S12**. Notably, the amount of decomposition products on the composite cathode increased in the order of NBR25 < NBR37 < PBD. As discussed earlier, the composite cathode with PBD has high resistance owing to the deterioration of interfacial contacts and the formation of numerous cracks in the active materials, resulting in a large overpotential during charging and the extension of the constant voltage charge at the end of charging. Therefore, a large amount of LPSCl was oxidatively decomposed on the composite cathode with PBD, which is another reason for the large capacity fading in the PBD cell.

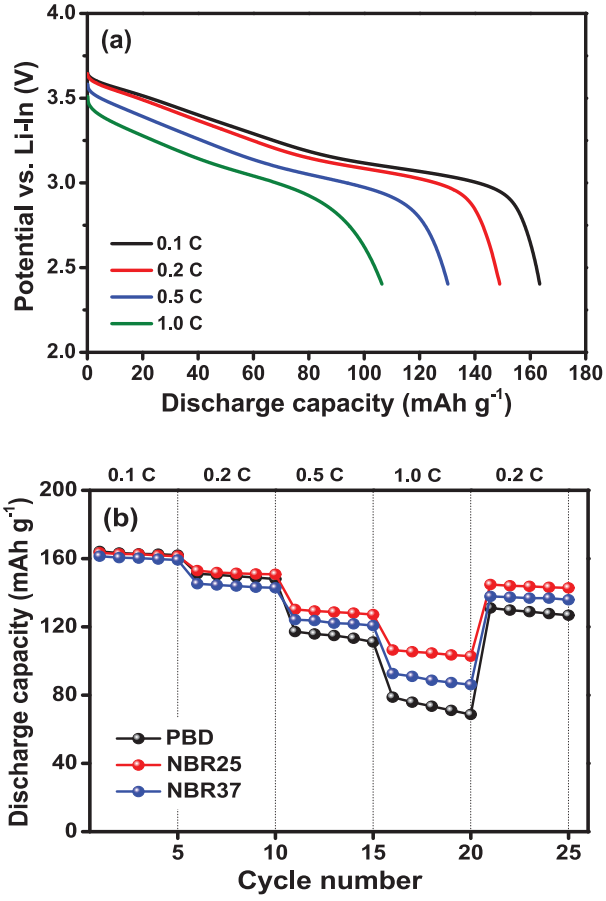

Fig. 6. (a) Discharge curves of all-solid-state cells prepared with NBR25 at different current rates and (b) discharge capacities of all-solid-state cells with different binders as a function of the current rate.

Fig. 6**a** shows the discharge curves of the solid-state Li-In/Li_6PS_5Cl/$LiNi_{0.7}Co_{0.1}Mn_{0.2}O_2$ cell employing the NBR25 binder at different current rates. With an increase in the current rate, the overpotential of the cell increased, along with a decrease in the discharge capacity. The cell exhibited a discharge capacity of 106.4 mAh g^{-1} at a current rate of 1.0 C and temperature of 25 °C. Fig. 6**b** shows a comparison of the discharge capacities of the cells with different binders at different current rates. The current rate was increased after every five cycles from 0.1 to 1.0 C and then decreased to 0.1 C. Notably, the differences in the discharge capacity increased with increasing current rate. The NBR25 cell delivered the highest discharge capacities at all the tested current rates, which was ascribed to the lowest cell resistance owing to the maintenance of good interfacial contacts in the NBR25-based composite cathode.

Conclusions

The composite cathode for ASSLBs was prepared with NCM712, solid electrolyte (LPSCl), conducting carbon, and different types of

polymer binders (PBD, NBR25, and NBR37) using a wet-slurry process. Mechanical and morphological analyses of the composite cathodes confirmed that NBR25 strongly adhered to NCM712 and LPSCl owing to the presence of nitrile groups and accommodated the mechanical stress caused by the large volume change of NCM712, thereby maintaining good interfacial contacts among the cathode components during repeated cycling. Accordingly, the all-solid-state lithium cell assembled with the composite cathode employing NBR25 exhibited the best cycling performance in terms of the cycling stability and high-rate performance. Our results demonstrate that the cycling performance of all-solid-state cells can be improved by appropriately selecting the polymer binder in the composite cathode.

Data availability

The authors do not have permission to share data.

Declaration of Competing Interest

The authors declare that they have no known competing financial interests or personal relationships that could have appeared to influence the work reported in this paper.

Acknowledgments

This study was supported by the National Research Foundation of Korea funded by the Korean government (2021R1A2C2011050) and the Technology Innovation Program (20012330) funded by the Ministry of Trade, Industry, and Energy (MOTIE, Korea).

Appendix A. Supplementary material

Supplementary data to this article can be found online at https://doi.org/10.1016/j.jiec.2023.02.034.

References

[1] F.W. Geels, Energy Res. Soc. Sci. 37 (2018) 224–231, https://doi.org/10.1016/j.erss.2017.10.010.
[2] J. Liang, J. Luo, Q. Sun, X. Yang, R. Li, X. Sun, Energy Storage Mater. 21 (2019) 308–334, https://doi.org/10.1016/j.ensm.2019.06.021.
[3] X. Lin, G. Zhou, J. Liu, J. Yu, M.B. Effat, J. Wu, F. Ciucci, Adv. Energy Mater. 10 (2020) 2001235, https://doi.org/10.1002/aenm.202001235.
[4] Y. Kato, S. Hori, T. Saito, K. Suzuki, M. Hirayama, A. Mitsui, M. Yonemura, H. Iba, R. Kanno, Nat. Energy 1 (2016) 16030, https://doi.org/10.1038/nenergy.2016.30.
[5] Z. Gao, H. Sun, L. Fu, F. Ye, Y. Zhang, W. Luo, Y. Huang, Adv. Mater. 30 (2018) 1705702, https://doi.org/10.1002/adma.201705702.
[6] Z. Cheng, T. Liu, B. Zhao, F. Shen, H. Jin, X. Han, Energy Storage Mater. 34 (2021) 388–416, https://doi.org/10.1016/j.ensm.2020.09.016.
[7] N. Kamaya, K. Homma, Y. Yamakawa, M. Hirayama, R. Kanno, M. Yonemura, T. Kamiyama, Y. Kato, S. Hama, K. Kawamoto, A. Mitsui, Nat. Mater. 10 (2011) 682–686, https://doi.org/10.1038/nmat3066.
[8] A. Sakuda, A. Hayashi, M. Tatsumisago, Sci. Rep. 3 (2013) 2261, https://doi.org/10.1038/srep02261.
[9] D. Chang, K. Oh, S.J. Kim, K. Kang, Chem. Mater. 30 (2018) 8764–8770, https://doi.org/10.1021/acs.chemmater.8b03000.
[10] S.-Y. Jung, R. Rajagopal, K.-S. Ryu, J. Ind. Eng. Chem. 95 (2021) 350–356, https://doi.org/10.1016/j.jiec.2021.01.009.
[11] M. Wang, Z. Peng, W. Luo, Q. Zhang, Z. Li, Y. Zhu, H. Lin, L. Cai, X. Yao, C. Ouyang, D. Wang, Adv. Sci. 7 (2020) 2000237, https://doi.org/10.1002/advs.202000237.
[12] A. Banerjee, X. Wang, C. Fang, E.A. Wu, Y.S. Meng, Chem. Rev. 120 (2020) 6878–6933, https://doi.org/10.1021/acs.chemrev.0c00101.
[13] Y.-G. Lee, S. Fujiki, C. Jung, N. Suzuki, N. Yashiro, R. Omoda, D.-S. Ko, T. Shiratsuchi, T. Sugimoto, S. Ryu, J.H. Ku, T. Watanabe, Y. Park, Y. Aihara, D. Im, I. T. Han, Nat. Energy 5 (2020) 299–308, https://doi.org/10.1038/s41560-020-0575-z.
[14] S.-B. Hong, Y.-J. Lee, U.-H. Kim, C. Bak, Y.M. Lee, W. Cho, H.J. Hah, Y.-K. Sun, D.-W. Kim, ACS Energy Lett. 7 (2022) 1092–1100, https://doi.org/10.1021/acsenergylett.1c02756.
[15] K. Lee, S. Kim, J. Park, S.H. Park, A. Coskun, D.S. Jung, W. Cho, J.W. Choi, J. Electrochem. Soc. 164 (2017) A2075–A2081, https://doi.org/10.1149/2.1341709jes.
[16] Y.J. Nam, D.Y. Oh, S.H. Jung, Y.S. Jung, J. Power Sources 375 (2018) 93–101, https://doi.org/10.1016/j.jpowsour.2017.11.031.
[17] D.Y. Oh, Y.J. Nam, K.H. Park, S.H. Jung, K.T. Kim, A.R. Ha, Y.S. Jung, Adv. Energy Mater. 9 (2019) 1802927, https://doi.org/10.1002/aenm.201802927.
[18] J. Ruhl, L.M. Riegger, M. Ghidiu, W.G. Zeier, Adv. Energy Sustainability Res. 2 (2021) 2000077, https://doi.org/10.1002/aesr.202000077.
[19] T. Ates, M. Keller, J. Kulisch, T. Adermann, S. Passerini, Energy Storage Mater. 17 (2019) 204–210, https://doi.org/10.1016/j.ensm.2018.11.011.
[20] R. Ruess, S. Schweidler, H. Hemmelmann, G. Conforto, A. Bielefeld, D.A. Weber, J. Sann, M.T. Elm, J. Janek, J. Electrochem. Soc. 167 (2020), https://doi.org/10.1149/1945-7111/ab9a2c.
[21] K. Heo, J. Lee, J. Im, M.Y. Kim, H.-S. Kim, D. Ahn, J. Kim, J. Lim, J. Mater. Chem. A 8 (2020) 22893, https://doi.org/10.1039/d0ta07347d.
[22] W. Zhang, D.A. Weber, H. Weigand, T. Arlt, I. Manke, D. Schroder, R. Koerver, T. Leichtweiss, P. Hartmann, W.G. Zeier, J. Janek, ACS Appl. Mater. Interfaces 9 (2017) 17835–17845, https://doi.org/10.1021/acsami.7b01137.
[23] G. Appetecchi, F. Croce, R. Marassi, L. Persi, P. Romagnoli, B. Scrosati, Electrochim. Acta 45 (1999) 23, https://doi.org/10.1016/S0013-4686 (99) 00190-5.
[24] L. Gong, M.H.T. Nguyen, E.S. Oh, Electrochem. Commun. 29 (2013) 45, https://doi.org/10.1016/j.elecom.2013.01.010.
[25] L. Luo, Y. Xu, H. Zhang, X. Han, H. Dong, X. Xu, C. Chen, Y. Zhang, J. Lin, ACS Appl. Mater. Interfaces 8 (2016) 8154, https://doi.org/10.1021/acsami.6b03046.
[26] B. Emley, Y. Liang, R. Chen, C. Wu, M. Pan, Z. Fan, Y. Yao, Mater. Today Phys. 18 (2021), https://doi.org/10.1016/j.mtphys.2021.100397.
[27] S.-Y. Lee, Y. Choi, S.-H. Kwon, J.-S. Bae, E.D. Jeong, J. Ind. Eng. Chem. 74 (2019) 216–222, https://doi.org/10.1016/j.jiec.2019.03.009.
[28] J. Kim, K. Park, Y. Cho, H. Shin, S. Kim, K. Char, J.W. Choi, Adv. Sci. 8 (2021) 2004290, https://doi.org/10.1002/advs.202004290.
[29] J. Oh, S.H. Choi, B. Chang, J. Lee, T. Lee, N. Lee, H. Kim, Y. Kim, G. Im, S. Lee, J.W. Choi, ACS Energy Lett. 7 (2022) 1374–1382, https://doi.org/10.1021/acsenergylett.2c00461.
[30] B. Son, M.-H. Ryou, J. Choi, T. Lee, H.K. Yu, J.H. Kim, Y.M. Lee, ACS Appl. Mater. Interfaces 6 (2014) 526–531, https://doi.org/10.1021/am404580f.
[31] J. Auvergniot, A. Cassel, J.-B. Ledeuil, V. Vallet, V. Seznec, R. Dedryvere, Chem. Mater. 29 (2017) 3883–3890, https://doi.org/10.1021/acs.chemmater.6b04990.
[32] J. Auvergniot, A. Cassel, D. Foix, V. Viallet, V. Seznec, R. Dedryvere, Solid State Ion. 300 (2017) 78–85, https://doi.org/10.1016/j.ssi.2016.11.029.
[33] K.H. Park, Q. Bai, D.H. Kim, D.Y. Oh, Y. Zhu, Y. Mo, Y.S. Jung, Adv. Energy Mater. 8 (2018) 1800035, https://doi.org/10.1002/aenm.201800035.
[34] S.H. Jung, U.-H. Kim, J.-H. Kim, S. Jun, C.S. Yoon, Y.S. Jung, Y.-K. Sun, Adv. Energy Mater. 10 (2020) 1903360, https://doi.org/10.1002/aenm.201903360.
[35] Y. Han, S.H. Jung, H. Kwak, S. Jun, H.H. Kwak, J.H. Lee, S.T. Hong, Y.S. Jung, Adv. Energy Mater. 11 (2021) 2100126, https://doi.org/10.1002/aenm.202100126.